Heliyon 10 (2024) e38823

Contents lists available at ScienceDirect

Heliyon

journal homepage: www.cell.com/heliyon

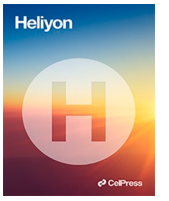

Research article

Identifying the signature of NAD+ metabolism-related genes for immunotherapy of gastric cancer

Huijuan Wen [a,b,1], Yang Mi [a,c,1], Fazhan Li [a,b,1], Xia Xue [a,c], Xiangdong Sun [a,b], Pengyuan Zheng [a,b,c,**], Simeng Liu [a,c,*]

[a] Henan Key Laboratory of Helicobacter pylori & Microbiota and Gastrointestinal Cancer, Marshall Medical Research Center, The Fifth Affiliated Hospital of Zhengzhou University, Zhengzhou, 450052, China
[b] Academy of medical science, Zhengzhou University, Zhengzhou, 450052, China
[c] Department of Gastroenterology, The Fifth Affiliated Hospital of Zhengzhou University, Zhengzhou, 450052, Henan, China

ARTICLE INFO

Keywords:
APOD
GC prognosis
Immunological biomarkers
Proliferation
Wnt/β-catenin/EMT signaling pathway

ABSTRACT

NAD (Nicotinamide Adenine Dinucleotide) -related metabolic reprogramming in tumor cells involves multiple vital cellular processes. However, the role of NAD metabolism in immunity and the prognosis of gastric cancer (GC) remains not elucidated. Here we identified and clustered 33 NAD + metabolism-related genes (NMRGs) based on 808 GC samples from the Cancer Genome Atlas (TCGA) and the Gene Expression Omnibus (GEO) databases. Survival analysis between different groups found a poor prognosis in the GC patients with high NMRGs expression. Gene *SGCE*, *APOD*, and *PPP1R14A* were identified and performed high expression in GC samples, while the qRT-PCR results further confirmed that their expression levels in GC cell lines were significantly higher than those from normal human gastric mucosa epithelial cells. Based on the single-cell analysis, Gene *SGCE*, *APOD*, and *PPP1R14A* can potentially be novel biomarkers of tumor-associated fibroblasts (CAFs). In parallel, the proliferation and migration of GC cells were significantly hampered following the knockdown of *SGCE*, *APOD*, and *PPP1R14A*, particularly *APOD*, we confirmed that *APOD* knockdown can inhibit β-catenin and N-cadherin expression, while promote E-cadherin expression. This study unveils a novel NMRGs-related gene signature, highlighting *APOD* as a prognostic biomarker linked to the tumor microenvironment. *APOD* drives GC cell proliferation and metastasis through the Wnt/β-catenin/EMT signaling pathway, establishing it as a promising therapeutic target for GC patients.

1. Introduction

Gastric cancer (GC) is the fifth most common tumor worldwide, and its incidence performs great geographic diversity [1]. East Asia reported the highest gastric cancer incidence rate at 0.0224 % among all continents in 2020 [2]. The 5-year survival rate of GC patients

* Corresponding author. Henan Key Laboratory of Helicobacter pylori & Microbiota and Gastrointestinal Cancer, Marshall Medical Research Center, The Fifth Affiliated Hospital of Zhengzhou University, Zhengzhou, 450052, China.
** Corresponding author. Henan Key Laboratory of Helicobacter pylori & Microbiota and Gastrointestinal Cancer, Marshall Medical Research Center, The Fifth Affiliated Hospital of Zhengzhou University, Zhengzhou, 450052, China.
E-mail addresses: pyzheng@zzu.edu.cn (P. Zheng), lsmxy66@163.com (S. Liu).
[1] These authors contributed equally to this work.

https://doi.org/10.1016/j.heliyon.2024.e38823
Received 29 June 2023; Received in revised form 3 September 2024; Accepted 30 September 2024
Available online 2 October 2024
2405-8440/© 2024 Published by Elsevier Ltd. This is an open access article under the CC BY-NC-ND license (http://creativecommons.org/licenses/by-nc-nd/4.0/).

Abbreviations

DEGs	differential genes
NMRGs	NAD + metabolism-related genes
TCGA	The cancer genome atlas project
GEO	Gene Expression Omnibus
KEGG	Kyoto Encyclopedia of Genes and Genomes
LASSO	Least Absolute Shrinkage and Selection Operator
TME	Tumor microenvironment
GSVA	Gene Set Variation Analysis
ROC:	Receiver operating characteristic curve
AUC	Area under the curve
OS	Overall survival
ssGSEA	Single sample gene set enrichment analysis
RNAss	Stemness score based on mRNA expression
TMB	Tumor mutation burden
MSI	Microsatellite instability
MSI-H:	Microsatellite instability-high
MSI-L:	Microsatellite instability – low
MSS	Microsatellite stability
PKM2	Pyruvate kinase's M2 subtype
ROS	Reactive oxygen species
CAFs	cancer-associated fibroblasts
CcRCC	Clear cell renal cell carcinoma

is lower than 20 % due to the lack of early GC diagnosis methods, efficient treatment techniques, and intervention targets [3–5], which can be benefited from the appropriate biomarkers for gastric carcinogenesis [6]. To date, the traditional biomarkers, including *CEA, CA125,* and *CA19-9*, have been clinically validated, although their efficiency and precision are somehow limited to a wide range of GC patients [7]. The positive diagnostic rates of *CEA*, *CA125*, and *CA19-9* in GC were reported as low as 4.4–21.1 %, 6.7–42.4 %, and 11.7–27.8 %, respectively [8–10]. It is therefore, urgent to find novel diagnostic markers that can be applied to the secondary prevention of GC.

Metabolic reprogramming plays a vital role in tumorigenesis, such as the Warburg effect [11]. It is closely related to the level of Nicotinamide Adenine Dinucleotide (NAD), which supports multiple critical cellular processes in tumors [12]. NAD is a crucial redox coenzyme in cellular metabolism in gluconeogenesis and the production of ketone and lipids [12]. NAD can be found in oxidized and reduced forms (NAD/NADH) from mitochondria. The imbalance of NAD/NADH homeostasis in mitochondria has been confirmed to be related to multiple human diseases, including cancer, heart failure, aging, Alzheimer's disease, Merger's disease, diabetes, and obesity [13–16]. Increased NAD levels have a protective effect on tumorigenesis at the early stage of tumors but convert into a detrimental factor at the late stage of tumor progression [17–19]. During cancer progression, increased NAD + levels can contribute to the tumor's malignancy process, which leads to rapid cell growth, increased resistance, and improved survival of tumors [20]. Previous studies have shown that targeting NAD + synthesis in GC cells can effectively inhibit energy and metabolite production [21].

Niacinate and nicotinamide metabolism could be involved in NAD + biosynthesis and degradation pathways [22]. Niacinate metabolism is associated with NAD + de novo and Preiss-Handler pathways, whereas nicotinamide metabolism is associated with NAD + salvage synthesis and NAD + depletion [23]. The genes related to NAD + metabolism (NMRGs) thus have been studied in human diseases, and their role in carcinogenesis would provide new strategies for cancer diagnosis and treatment [24]. NMRGs have been confirmed to be a risk factor for ovarian cancer (OC), and the expression of NMRGs showed a negatively correlated with the level of immune cell infiltration in OC patients, which can be related to the poor prognosis of patients [25]. Previous studies have shown that the immune microenvironment plays an essential role in cancer development. The prognosis of cancer patients with the same histological type was also affected by other immune cell infiltration [26]. Continuous communication has been found between GC cells and their surrounding environments. The complex tumor microenvironment (TME) of GC includes fibroblasts, immune cells, adipocytes, vascular endothelial cells, and extracellular matrix [27,28]. However, rare studies on the relationship between NMRGs, the prognosis, and the immune infiltration of GC patients have been raised.

APOD is a plasma high-density lipoprotein (HDL)-related glycoprotein with a putative role in the cholesterol (CHOL) transport pathway [29]. Significant downregulation of *APOD* is observed in hepatocellular carcinoma, colorectal cancer, epithelial ovarian cancer, and breast cancer, and its close association with tumor progression and poor prognosis in these cancer types has been reported [30–33]. However, the specific mechanisms pertaining to *APOD* and GC cells proliferation, migration and related pathways remain unclear.

This study aimed to investigate the relationship between the expression of NMRGs and the prognosis and immune infiltration of GC patients, based on bioinformatics analysis. Furthermore, *in vitro* experiments were conducted to verify the molecular mechanisms by which NMRGs, particularly *APOD*, affect the proliferation and migration of GC cells. A prognostic model has been constructed through

the Least Absolute Shrinkage and Selection Operator (LASSO) regression analysis. The association between risk score and tumor tissue immune cell infiltration, gene mutation, and tumor stemness score was explored given this model. *APOD* and the proliferation, migration and related mechanisms of GC cells were studied.

2. Results

2.1. Consistent clustering

To understand the roles of NMRGs and their related genes in GC, 33 overlapping NMRGs were used to perform consistent clustering of GC samples. The results showed that the most appropriate grouping (Criterion: there was the most significant difference between groups and the slightest difference within groups) was achieved when the samples were divided into 3 clusters (Fig. 1a and b). The survival analysis of the three cluster samples showed that the GC patients of cluster C with the lower expression of NMRGs showed better survival times (Fig. 1c). This result revealed that NMRGs were associated with the prognosis of GC patients and prompted us to explore the underlying mechanisms further.

2.2. GSVA pathway enrichment analysis

The relationship of differentially expressed NMRGs between different clusters and clinical information is shown in a heatmap. In cluster C, the expression levels of 19 NMRGs were significantly lower than those in cluster A ($P < 0.05$). We conducted the Gene Set Variation Analysis (GSVA) to explore the biological characteristics among these three distinct clusters. The results showed that the enrichment of glycosaminoglycan biosynthesis of chondroitin sulfate, ECM receptor interactions, and focus adhesion signaling pathways in the high NMRGs expression group was significantly higher than in the low NMRGs expression group ($P < 0.05$)(Supplementary Fig. S1).

2.3. Construction of risk models

To screen out the prognostic-related hub genes, we intersected the differential genes among the three clusters and obtained 27

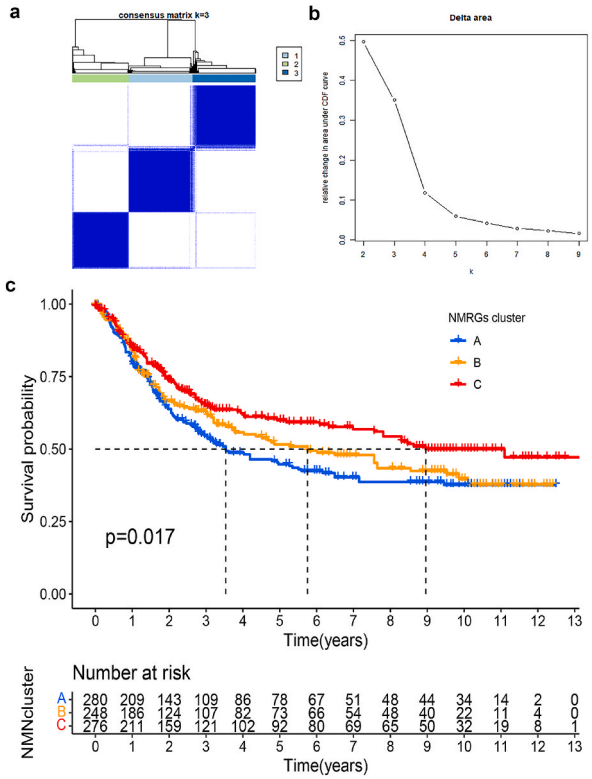

Fig. 1. Consistent cluster analysis. (a) When k = 3, GC samples can be best discriminated based on NMRGs. (b) The relative change of the area under the CDF curve is the largest when the consensus matrix k is from 3 to 4. (c) The blue line represents the cluster with higher expression of NMRGs; the yellow line represents the cluster with median NMRGs expression; the red line represents the cluster with lower NMRGs expression and survival analysis showed that GC patients from cluster C with the lower expression of NMRGs had better survival time ($P < 0.05$).

DEGs for the following analysis (Supplementary Fig. S2). LASSO regression analysis was conducted to identify *SGCE*, *APOD*, and *PPP1R14A* for constructing the prognostic model (Fig. 2a and b). The risk score was calculated based on the corresponding Cox regression model coefficients. Based on hub genes risk scores, the GC samples were divided into high-risk and low-risk groups. The results showed that GC patients in the low-risk group had better overall survival (OS) compared with the high-risk group (Fig. 2c), and the area under the ROC curve (AUC) for the OS of one year, three years, and five years were all greater than 0.5, indicating the reliability of the model (Fig. 2d).

By integrating multiple clinical factors and risk scores, we constructed a nomogram of GC patients and used a calibration curve to verify the accuracy of the nomogram. The results showed that risk score, age, and N stage were valuable for GC patients' prognosis, and the calibration curve similarly demonstrated the model's accuracy (Fig. 3a and b).

2.4. Immune infiltration of the tumor microenvironment

To explore differences in immune cell infiltration between the high-risk and low-risk groups, we quantified the level of immune infiltration in GC patients. We observed that the patients from the low-risk group obtained a lower estimate score, immune score, and stromal score than those from the high-risk group (Fig. 4a). Combining with different clusters, we further explored the relationship between the expression of *SGCE*, *APOD*, and *PPP1R14A* and various immune cells, and the results showed that follicular helper T cells and CD4 memory-activated T cells were negatively correlated with the expression levels of the three hub genes, while CD4 memory-resting T cells, Monocytes and resting Mast cells were positively correlated (Fig. 4b and c). We found that *SGCE*, *APOD*, and *PPP1R14A* were positively correlated with 22 differential NMRGs, among which *AOX1* and *PTGIS* showed the strongest correlation with NMRGs (Supplementary Fig. S3). Survival analysis in GC samples showed that the low expression of *SGCE*, *APOD*, and *PPP1R14A* was associated with better prognosis of patients (Supplementary Fig. S4).

2.5. Correlation of risk scores with GC mutational status and microsatellite instability

The low-risk group showed a higher mutation rate than the high-risk group, and among the top 20 driver mutation genes, *TTN* and *TP53* carried the highest mutation rates (Fig. 5a and b). The evidence indicated that patients with higher TMB had a better response to immunotherapy and thus performed a better prognosis than patients with lower TMB. TMB score was lower in the high-risk group than in the low-risk group (Fig. 5c). Tumor stemness analysis showed that stemness score based on mRNA expression (RNAss) was inversely correlated with risk score (Fig. 5d). Microsatellite stability status differed in GC patients, and the patients' effect on immunotherapy varied. Risk scores significantly differed among the different microsatellite stability status groups ($P < 0.05$) (Fig. 5e). The proportion

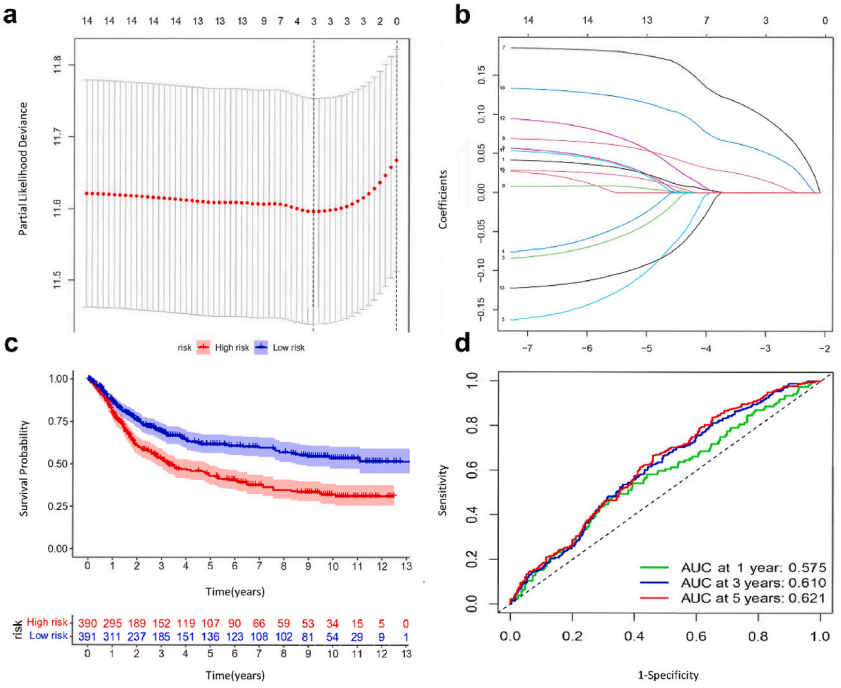

Fig. 2. LASSO regression analysis to construct a prognostic model. (a&b) Three genes significantly associated with the overall survival of GC patients were identified by LASSO regression analysis. (a) Ten-fold cross-validation was used to select the best parameters (lambda). (b) Optimal lambda determined the LASSO coefficient distribution. (c) Survival curve between the high-risk group and low-risk group. (d) The area under the ROC curve (AUC) for the OS of one year, three years, and five years.

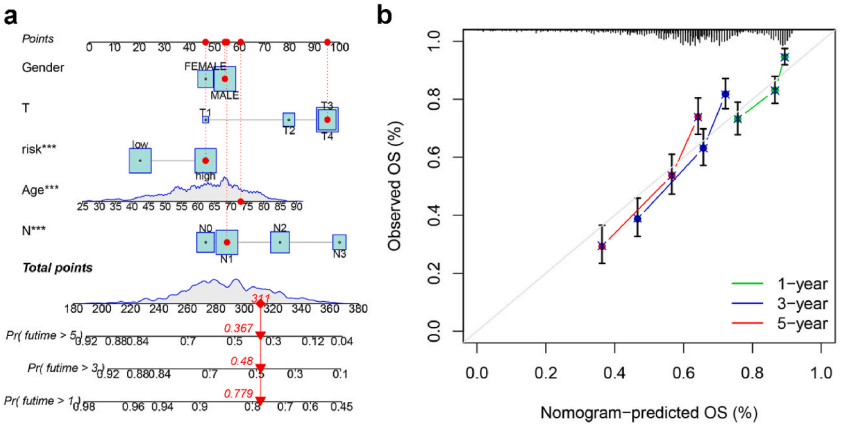

Fig. 3. The nomogram model of GC patients and the model's calibration curves. (a) Prognostic nomogram for predicting 1-, 3-, and 5-year survival probabilities in GC patients. (b) Calibration curves of 1-, 3-, and 5-year overall survival predicted by the nomogram. The X-axis is the predicted survival probability of the nomogram, and the Y-axis is the observed survival probability. The solid red, green, and blue lines represent the performance of the column lines relative to the 45-degree line, indicating perfect predictions. *, $P < 0.05$; **, $P < 0.01$; ***, $P < 0.001$.

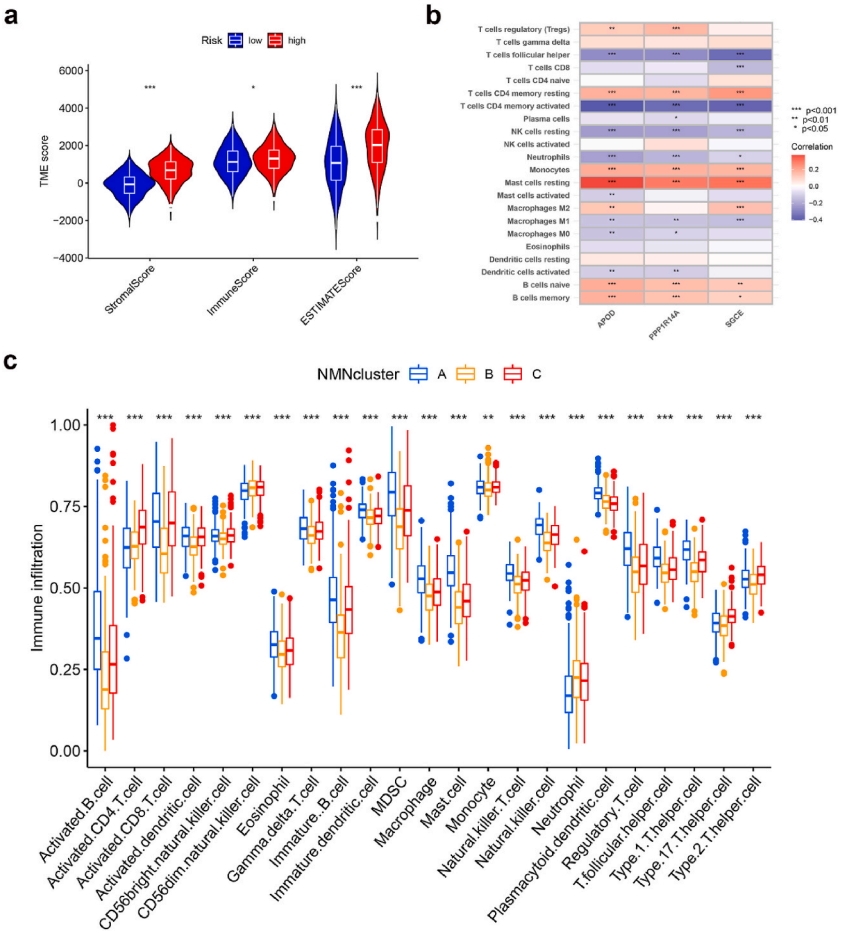

Fig. 4. TME characteristics. (a) The TME scores between different risk subgroups. Blue represents the low-risk group and red represents the high-risk group. (b) Heatmap of the correlation between different genes and immune cells. Red represents positive correlation and blue represents negative correlation. The darker the color, the stronger the correlation. (c) The relationship between the expression level of NMRGs and immune cell infiltration. The blue frame represents the cluster with higher expression of NMRGs; the yellow box represents the cluster with median-NMRGs expression; and the red rectangle represents the cluster with lower NMRGs expression. *, $P < 0.05$; **, $P < 0.01$; ***, $P < 0.001$.

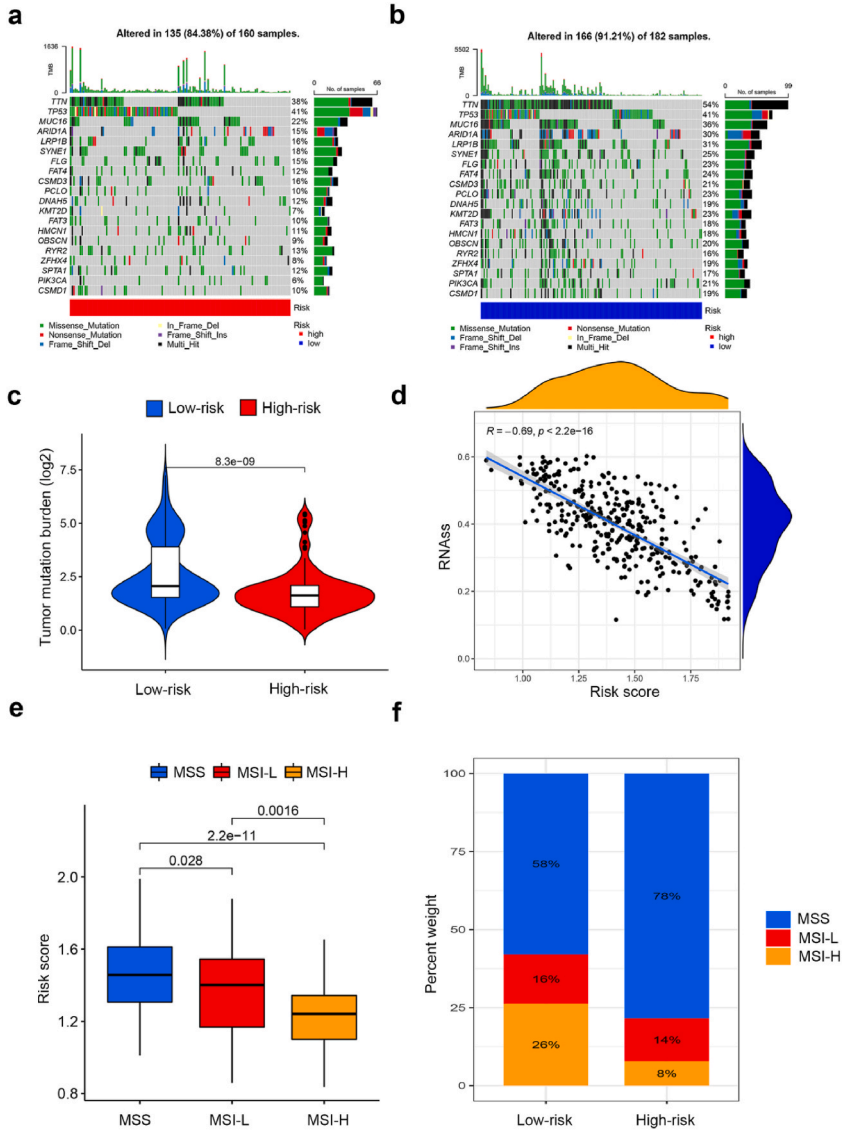

Fig. 5. Correlation of risk score with TMB, RNAss, and MSI in GC. (a&b) Frequency of somatic mutations in GC patients in two risk subgroups. Red represents the high-risk group, and blue represents the low-risk group. (c) Differences in TMB scores between different risk groups. (d) Association of risk scores with RNAss. (e) Risk scores among different microsatellite status subgroups. Blue represents the microsatellite stable (MSS) group, red represents the microsatellite instability-low (MSI-L) group, and yellow represents the microsatellite instability-high (MSI-H) group, the numbers above the graphs represent *P*-values. (f) Proportions of different microsatellite stability states in different risk subgroups, the numbers in the figure represent the percentages of different samples.

(42 %) of microsatellite instability-high (MSI-H) and microsatellite instability-low (MSI-L) in the low-risk subgroup was higher than that (22 %) in the high-risk subgroup (Fig. 5f).

2.6. Gene signature and CAFs

We analyzed the single-cell RNA sequencing data of primary and metastatic gastric cancer tissues of 6 patients, and combined 10 samples, which were performed batch effects and cell clustering (Supplementary Fig. S5). Through the singleR database and looking at the classic cell markers, we found that *SGCE*, *APOD*, and *PPP1R14A* were mainly expressed in tumor-associated fibroblasts (CAFs) (Fig. 6a and b). *SGCE*, *APOD*, and *PPP1R14A* were highly consistent with the expression of CAFs classic markers in cells (the CAFs markers used for identification were *ACTA2*, *FAP*, *PDGFRA*, *PDGFRB*, *PDPN*, *THY1*, and *COL1A1*) (Fig. 6c and d), which means that these three genes can also serve as markers for CAFs. Finally, we quantified and scored the transcriptome samples through CAFs markers to verify the relationship between *SGCE*, *APOD*, and *PPP1R14A* and CAFs. The results showed that the CAFs content was

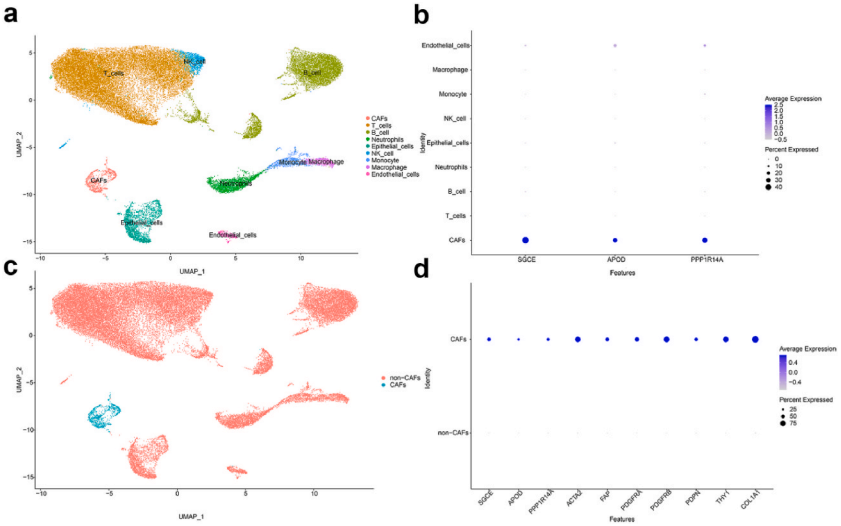

Fig. 6. Identification of *SGCE*, *APOD*, and *PPP1R14A* in cells. (a) Cell type identification of tumor cells. (b) Expression distribution of *SGCE*, *APOD*, and *PPP1R14A* in cells. (c&d) Consistent identification of gene signatures (*SGCE*, *APOD*, and *PPP1R14A*) and CAFs markers (*ACTA2*, *FAP*, *PDGFRA*, *PDGFRB*, *PDPN*, *THY1* and *COL1A1*) expressed by CAFs and non-CAFs cells in tumors.

higher in the high-risk group samples (Fig. 7a), and similarly, the correlation heatmap also showed that *SGCE*, *APOD*, and *PPP1R14A* and risk score are significantly positively correlated with CAFs markers and *AOX1* and *PTGIS*. (Fig. 7b). Finally, the results of the survival curve showed that gastric cancer patients with fewer CAFs had a better prognosis (Fig. 7c). Based on the gene signature risk score, it was found that patients with fewer CAFs combined with a low-risk score had the best prognosis (Fig. 7d). These results imply that *SGCE*, *APOD*, and *PPP1R14A* may function mainly by regulating CAFs.

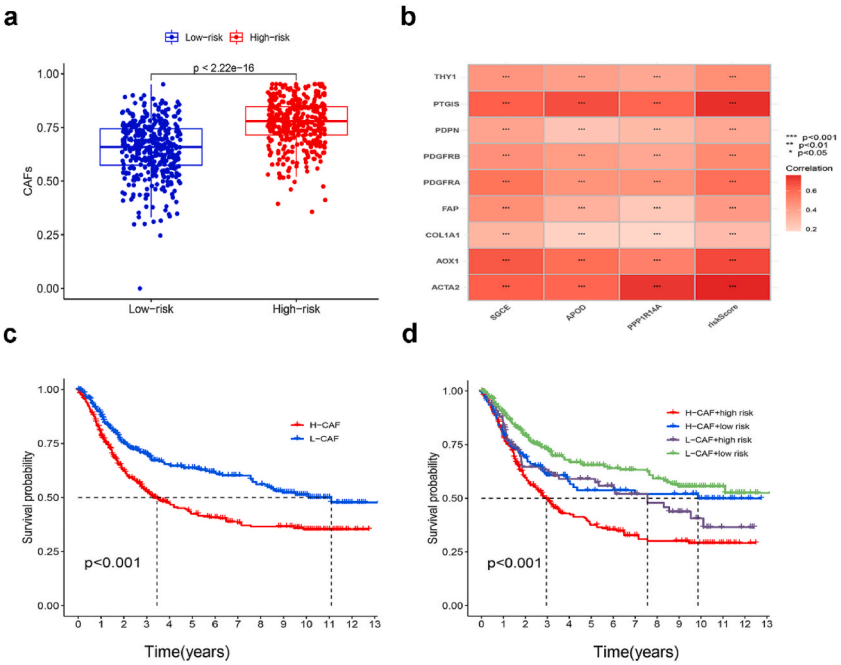

Fig. 7. Relationship between risk score and CAFs. (a) Comparison of CAFs content in high-risk and low-risk samples. (b) Correlation heatmap of *SGCE*, *APOD*, and *PPP1R14A* with CAFs markers, *AOX1* and *PTGIS* in NMRGs. (c) Survival analysis of CAFs-associated gastric cancer patients. (d) The effect of risk score combined with CAFs on the prognosis of gastric cancer patients.

2.7. qRT-PCR

To further determine the expression of *SGCE*, *APOD*, and *PPP1R14A* in GC cell lines and normal gastric mucosa epithelial cells, we conducted qRT-PCR to examine the expression of *SGCE*, *APOD*, and *PPP1R14A* in normal human gastric mucosa epithelial cell and five GC cells. The results showed that the expression levels of *SGCE*, *APOD*, and *PPP1R14A* in GC cell lines were on average 3-fold, 7-fold, and 5-fold higher than that in normal human gastric mucosa epithelial cell, respectively ($P < 0.05$) (Fig. 8), which were consistent with our previous analysis.

2.8. The relationship between APOD, PPP1R14A and SGCE and proliferation of gastric cancer cells

To assess the knockdown efficiency of *APOD*, *PPP1R14A*, and *SGCE*, RNA interference was performed using two cell lines SGC-7901 and AGS. It was observed that *APOD* showed the highest knockdown efficiency (≥80 %) as determined by qRT-PCR (Fig. 9). It was evidenced the proliferation activity of SGC-7901 (Fig. 10a–c) and AGS cells (Fig. 10d–f) was reduced after knocking down *APOD*, *PPP1R14A* and *SGCE* through CCK8 experiment. Furthermore, in comparison to the other two genes, the knockdown of *APOD* resulted in the lowest proliferation activity among gastric cancer cells.

2.9. APOD affects the proliferation and migration of gastric cancer cells

To further validate the inhibitory effect of *APOD* on the proliferation of GC cells, plate cloning experiments were conducted in SGC-7901 and AGS cells (Fig. 11a). In comparison to the control group, the number of colonies in the *APOD* knockdown group was significantly reduced, particularly in the si-APOD-#3 group (Fig. 11b). In wound healing experiments, it was determined that the migration ability of SGC-7901 and AGS cells was significantly inhibited upon the knockdown of *APOD* (Supplementary Fig. 6).

2.10. The knockdown of APOD inhibits the proliferation of gastric cancer cells through the Wnt/β-catenin/EMT signaling pathway

APOD, N-caderin and β-catenin were highly expressed, while E-caderin was lowly expressed in AGS and SGC-7901 cells compared with normal human gastric mucosa epithelial cells (Fig. 12a), and the differences were statistically significant (Fig. 12c). The GC cells was most significantly inhibited utilizing si-APOD-#3, we thus investigate the pathways associated with *APOD*-mediated promotion of GC cells proliferation in AGS and SGC-7901 (Fig. 12b). There was a significant reduction in the expression of N-cadherin and β-catenin, while the expression of E-cadherin was increased following the knockdown of *APOD* (Fig. 12d). This indicates that *APOD* leads to GC cells proliferation through the Wnt/β-catenin/EMT signaling pathway.

3. Discussion

This study found that GC patients with a low expression level of NMRGs showed a higher survival time generally, potentially indicating that the expression level of NMRGs acts as a detrimental factor in GC progression. The increased NAD with the assistance of pyruvate kinase's M2 subtype (PKM2), can effectively improve the redox capacity of tumor cells and thus protect against reactive oxygen species (ROS)-induced damage [34,35], as well as reduce the occurrence of apoptosis. Moreover, increased NAD leads to increased PARP1-dependent poly-ADP nucleation, thereby promoting tumorigenesis, in parallel, its increase raises the activity of sirtuin to promote tumor cell growth [13]. The pathway enrichment analysis of GSVA also showed that the enrichment of glycosaminoglycan biosynthesis of chondroitin sulfate, ECM receptor interactions, and focus adhesion signaling pathways in GC samples with high NMRGs expression was significantly higher than in the group with low NMRGs expression ($P < 0.05$), which may be the reason why the expression of NMRGs promote the progression of GC. It has been found that glycosaminoglycan

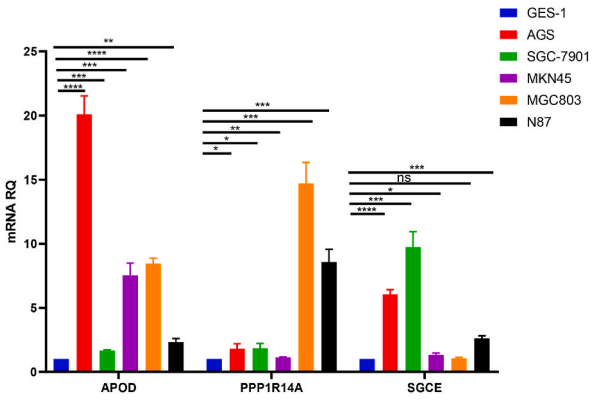

Fig. 8. Relative expression of *SGCE*, *APOD*, and *PPP1R14A* in GES-1 cell and five GC cell lines N87, SGC7901, MKN45, AGS, and MGC803. ns, no significance; *, $P < 0.05$; **, $P < 0.01$; ***, $P < 0.001$; ****, $P < 0.0001$.

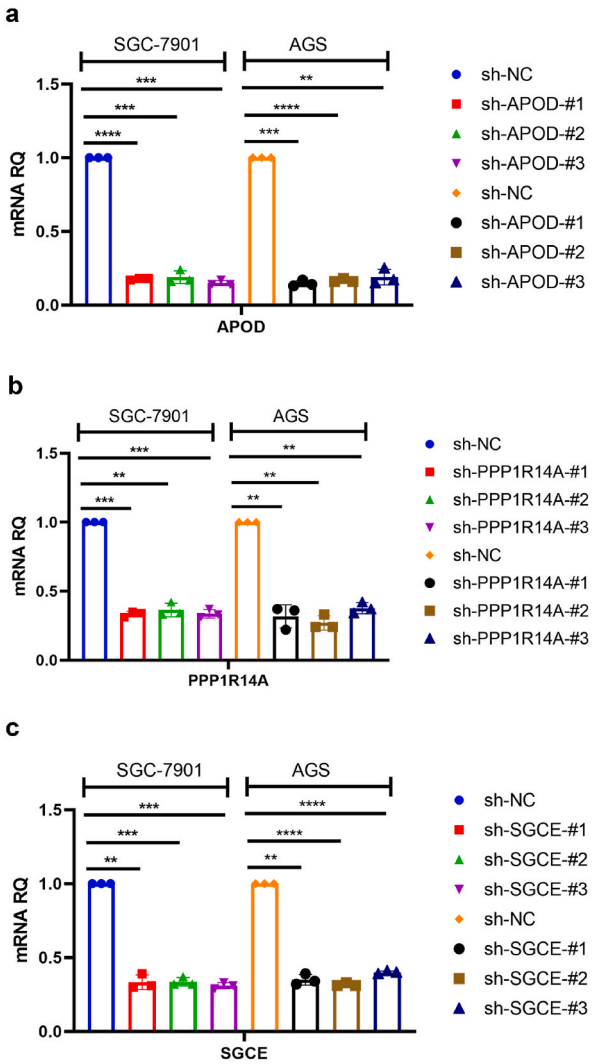

Fig. 9. The expression of *APOD*, *PPP1R14A* and *SGCE* among gastric cancer and cells knocked down the corresponding genes. **, $P < 0.01$; ***, $P < 0.001$; ****, $P < 0.0001$.

biosynthesis-chondroitin sulfate metabolic reprogramming was associated with poor prognosis in GC patients [36], and ECM receptor interaction and focal adhesion were significantly activated in GC patients from the high-risk group [37].

In the analysis of immune cell tumor infiltration, we found resting Mast cells and CD4 memory resting T cells significantly positively correlated with NMRGs, and CD4 memory activated T cells significantly negatively correlated ($P < 0.001$). The novel CAFs markers of GC, SGCE, APOD, and PPP1R14A, were identified and the GC patients with high-CAFs have a worse prognosis. Relevant studies have shown that the increased infiltration level of resting Mast cells that may act synergistically with CAFs in GC patients is associated with poor prognosis of patients [38,39]. CAFs remodel the extracellular matrix (ECM) and lead to the collective invasion of tumor cells, creating a supportive niche for cancer stem cells, weakening the tumor immune microenvironment (TIME), and reprogramming cancer cell resting metabolism, in the promotion of tumor metastasis and immune escape [40–42].

The infiltration of CD4 cells plays a vital role in the immune micro-environment of tumors and can significantly affect the prognosis of patients [43]. In colon cancer, an increase in CD4 memory-resting T cells has been identified as a risk factor, whereas CD4 memory-activated T cells play a protective role [44]. These results suggest that NMRGs may regulate CAFs through *SGCE*, *APOD*, and *PPP1R14A*, which in turn modulate the immune microenvironment in GC, ultimately affecting patients' prognosis. This result indicates that the effect of NMRGs on GC may mainly depend on the synergistic effect of *AOX1* and *PTGIS* with *SGCE*, *APOD*, and *PPP1R14A*. High expression of *PTGIS* has been reported to be associated with poor overall survival and progression-free survival in GC [45]. The high expression of *AOX1* in liver cancer can promote tumor proliferation [46], while its high expression in prostate cancer and clear cell renal cell carcinoma (ccRCC) [47,48] can inhibit tumor cells.

TMB and MSI are closely related to the prognosis after immunotherapy in multiple tumors and can be used as biomarkers to predict the effect of immunotherapy [49]. Our analysis showed that TMB was significantly lower in the high-risk group than in the low-risk

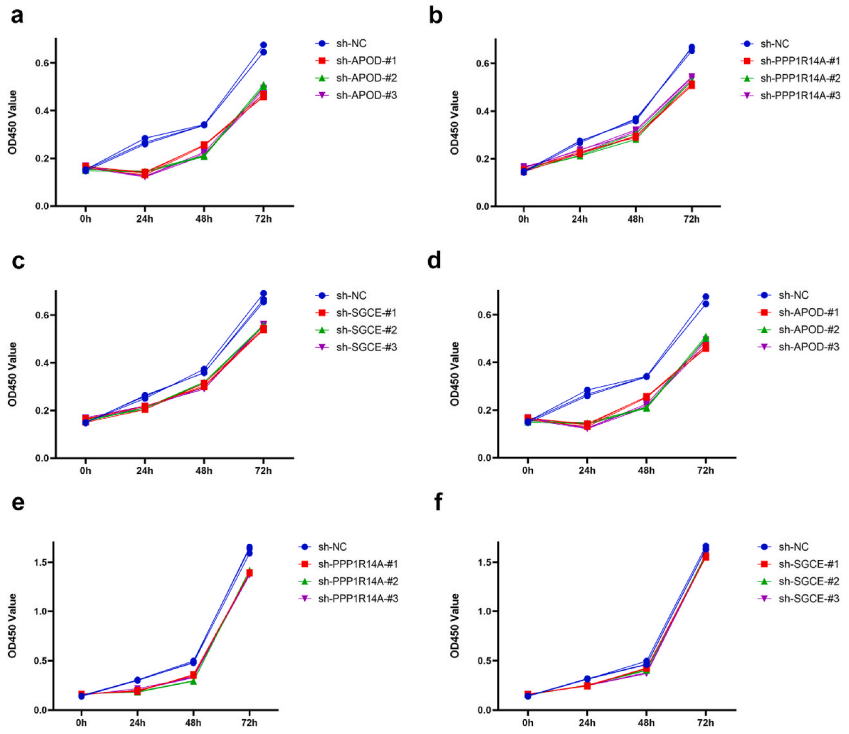

Fig. 10. The effects of *APOD*, *PPP1R14A* and *SGCE* on GC cell proliferation. (a–c) The proliferation of SGC-7901 cells after the knockdown of *APOD*, *PPP1R14A*, and *SGCE* by CCK8 assay. (d–f) The proliferation of AGS cells following knockdown of *APOD*, *PPP1R14A*, and *SGCE* in CCK8 experiment.

group ($P < 0.05$), and the proportion of MSI-H and MSI-L in the low-risk group was higher than in the high-risk group. Patients with high TMB levels showed significantly better tumor remission and survival after nivolumab treatment than those with low TMB levels [50]. A multicenter meta-analysis reported that patients with MSI were more likely to benefit from treatment than patients with microsatellite stability (MSS) in GC [51]. Furthermore, we found that risk scores were significantly negatively correlated with RNAss in GC, which suggests that the stemness of tumor cells in the low-risk group is higher than in the high-risk group. In GC patients, the group with high RNAss has a higher incidence of MSI and a lower pathological stage than that with low RNAss. The group with high RNAss can achieve better chemotherapy response and, thus, a better prognosis [52].

We employed GC cell lines to validate the roles of *SGCE*, *APOD*, and *PPP1R14A*. Our findings revealed that the knockdown of these three genes in GC cell lines led to discernible differences in cellular phenotypes. Specifically, the suppression of *SGCE*, *APOD*, and *PPP1R14A* significantly impeded tumor cell proliferation (Fig. 10). Notably, *APOD* showed a higher inhibitory effect on tumor cell migration compared with *SGCE* and *PPP1R14A*. We further explored the effect of *APOD* knockdown on GC migration and the specific molecular mechanisms that affect GC proliferation and migration. Epithelial–mesenchymal transition (EMT) is recognized as a pivotal process in cancer metastasis, thus the relationship of *APOD* and EMT in GC cells was studied. EMT facilitates the dissemination of cells from the primary tumor, enabling epithelial-like tumor cells (cancer cells) to acquire invasive mesenchymal-like traits [53]. Various stromal cell-derived signals, including paracrine signals from CAFs, orchestrate and sustain EMT in the primary tumor [54]. Up to now, there are still lack of reports related to *APOD* and tumor metastasis. In our current investigation, we demonstrated that downregulation of the gastric CAFs marker *APOD* impedes the EMT process in tumor cells, resulting in reduced tumor cell migration. This novel finding suggests that *APOD*, as a marker of gastric CAFs, may plays a pivotal role in mediating the crosstalk between tumor cells and the tumor microenvironment (TME) by regulating EMT events in tumor cells.

However, it is essential to acknowledge the limitations of our study. The ROC value of the risk model based on the gene signature did not meet optimal standards (0.8). In parallel, further animal experiments and the collection of more clinical samples are needed to validate these preliminary results. In summary, we preliminary revealed the correlation between NMRGs and prognosis in GC patients for the first time and identified genes *SGCE*, *APOD*, and *PPP1R14A*, which cooperate with NMRGs. The oncogenic properties of *APOD*, encompassing the promotion of proliferation and migration in GC cells through the Wnt/β-catenin/EMT signaling pathway, were meticulously validated. These findings suggest that a gene signature consisting of these three genes, especially *APOD* can serve as an effective predictor of GC treatment outcomes.

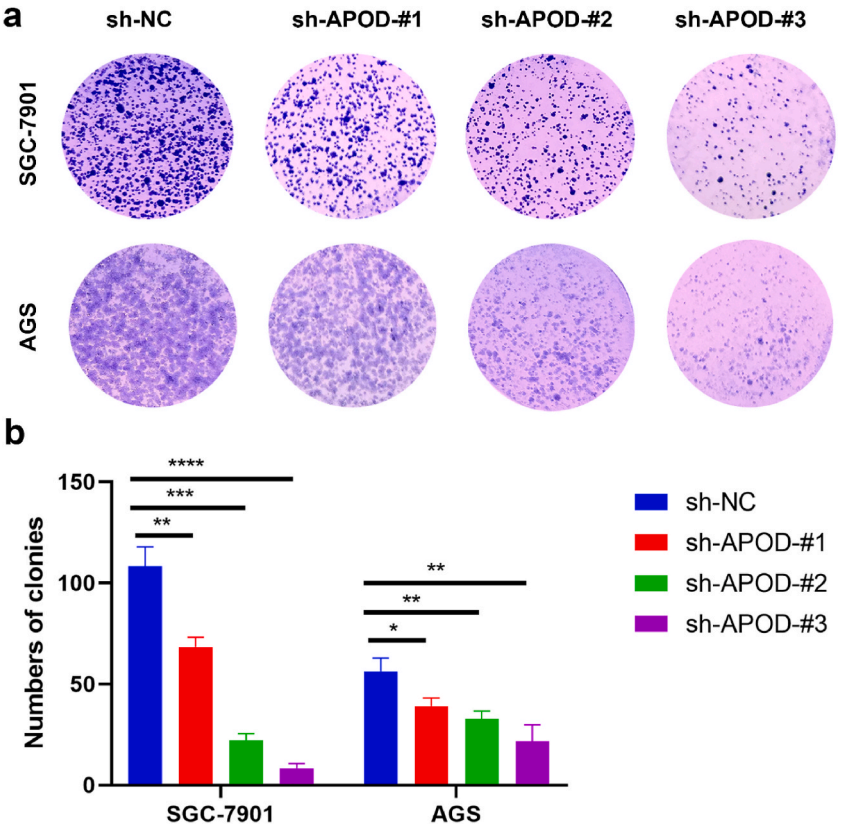

Fig. 11. The influence of knocking down *APOD* on cell colony formation on SGC-7901 and AGS cells. (a) The photo showing the number of clones formed by SGC-7901 and AGS cells after knocking down APOD. (b) The visual analysis of the number of clones formed by SGC-7901 and AGS cells after knocking down APOD through plate cloning experiments. *, $P < 0.05$; **, $P < 0.01$; ***, $P < 0.001$; ****, $P < 0.0001$.

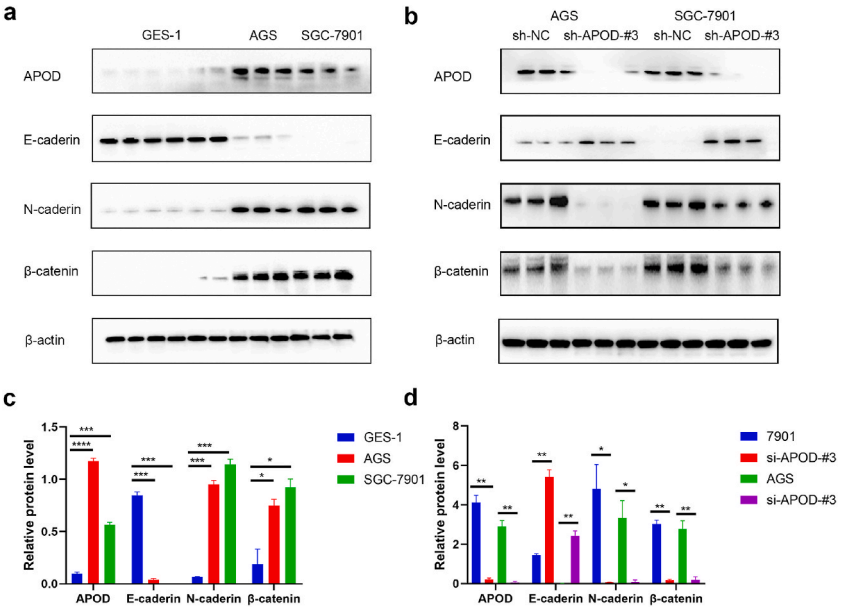

Fig. 12. The expression of Wnt/β-catenin/EMT signaling pathway-related proteins among different cells. (a&c) The expression of Wnt/β-catenin/EMT signaling pathway-related proteins among AGS, SGC-7901 and GES-1 cells. (b&d) The expression of Wnt/β-catenin/EMT signaling pathway-related proteins following knocking down *APOD* in AGS and SGC-7901 cells. *, $P < 0.05$; **, $P < 0.01$; ***, $P < 0.001$; ****, $P < 0.0001$.

4. Methods and materials

4.1. Data collection

Complete gene expression data, clinical information, and mutation data (including 375 GC samples and 32 normal gastric tissue samples) from the TCGA online database (https://portal. gdc. cancer. gov/) were downloaded. The RNA-seq data for 19,505 genes were measured as fragments per kilobase of transcript per million mapped reads (FPKM), which were converted to transcripts per million (TPM) after removing duplicated genes and zero expression genes [55]. In addition, the GSE84437 dataset [56] with a total of 433 GC samples sequencing data from the Gene Expression Omnibus (GEO, https://www. ncbi. nlm. nih. gov/geo/database) online database was also downloaded. The TCGA-STAD and GSE84437 [56] data were batches corrected by using the "limma" package [57] and "sva" package [58] and were merged. The normal samples in TCGA-STAD were removed and the remained ones were merged with the GC samples in GSE84437. Thus 808 GC samples were obtained after eliminating the batch effect. The GSE163558 [59] single-cell data set includes, ten tissues of different organs or tissues (primary gastric cancer PT1, primary gastric cancer PT2, primary gastric cancer PT3, adjacent non-tumoral NT1, gastric cancer lymph node metastasis LN1, gastric cancer lymph node metastasis LN2, gastric cancer ovary metastasis O1, gastric cancer peritoneum metastasis P1, gastric cancer liver metastasis Li1, gastric cancer liver metastasis Li2) from six patients, with a total of 96810 cells [59]. NAD + metabolism-related genes (NMRGs) were obtained from the Kyoto Encyclopedia of Genes and Genomes (KEGG) pathway database (Pathway: hsa00760) and Reactome database (R-HSA-196807). The 33 overlapping NMRGs between the above database and TCGA-STAD and GEO-STAD datasets were identified.

4.2. Consistent clustering

The "ConsensusClusterPlus" package [60] was performed based on the 33 overlapping NMRGs utilized for consistent clustering to determine subgroups of GC samples. The Euclidean squared distance metric and the K-means clustering algorithm were used for classifying samples into k clusters with $k = 2$ to $k = 9$. The results were presented using the "pheatmap" package [61], and the optimal number of clusters was determined by the consistent cumulative distribution function (CDF) graph and the delta region graph [62]. In addition, the "pheatmap" package [61] and the "survival" package [63] were used to separately draw the heatmap of the relationship between different clusters and patient clinical information and survival curves between samples of each cluster.

4.3. GSVA enrichment analysis

GSVA was performed to evaluate the pathways enriched in each cluster with the R package "GSVA" and "c2. cp. kegg. v7. 4. symbols" from the Molecular Signatures Database (MSigDB) [64]. Significance was defined according to a normalized $P < 0.05$.

4.4. LASSO regression analysis

The "limma" package was used to identify differential genes among different clusters (The adjusted $P < 0.05$ and the absolute value of Log_2 fold change >0.585 were used as screening criteria) [65] and the "VennDiagram" package [66] was applied to draw Venn diagrams. To further identify gene sets more relevant to the prognosis of GC, univariate Cox regression analysis was processed to screen out genes that were valuable for the prognosis of GC patients ($P < 0.05$), and the most minor absolute shrinkage and selection operator (LASSO) Cox regression analysis was made to construct a prognostic gene signature with R package "glmnet" [67]. By combining the weighted regression coefficients on gene expression, GC samples were divided into high-risk and low-risk groups. The survival curves were drawn for different risk models based on the "survival" package [63]. The time-dependent receiver operating characteristic (ROC) curve was plotted, and the area under the ROC curve (AUC) was also calculated with the R package "timeROC" [68]. All independent prognostic factors were used to build a nomogram to evaluate the 1-, 3-, and 5-year survival probability for patients with GC [69].

4.5. Immune cell infiltration analysis

Single-sample Gene Set Enrichment Analysis (ssGSEA) was conducted to quantify the relative abundance of each immune cell in the TME and the immune-related gene set was obtained with the R package "GSVA" [70], the "ggplot2" package [71] was applied to visualize the immune cell infiltration between different clusters. The "CIBERSORT" package [72] was utilized to analyze gene expression information in GC samples and to estimate the abundance of 22 different immune cell subsets. Besides, the Expression Data algorithm [73] was employed to estimate stromal cells and immune cells in GC. The unique properties of the transcriptomic profiles were fully utilized to infer the tumor cellularity and purity.

4.6. Correlation of risk scores with GC mutational status and microsatellite instability

The Masked Somatic Mutation data were obtained, analyzed, and visualized using the "maftools" package [74]. The mutation differences between the high-risk and low-risk groups were displayed in waterfall plots. Tumor mutation burden (TMB) variance analysis and correlation analysis were further performed for different risk groups. In addition, the correlation of different risk groups with microsatellite instability (MSI) was also explored and plotted as boxplots. In this study, tumor stemness scores were obtained

based on mRNA expression (RNAss) using the calculation method in the previous studies [75]. The expression data was integrated with the stemness score for the Spearman correlation test.

4.7. Single-cell data processing and dimensionality reduction

The gastric cancer sequencing data of GSE163558 from the GEO database were downloaded (https://www.ncbi.nlm.nih.gov/geo/query/acc.cgi?acc=GSE163558), which included single-cell sequencing data from tumor samples of six gastric cancer patients. The sequencing data of the tumor tissue were extracted and the Seurat package in R software was used to create processable objects [76]. For each sample, the gene and count features were identified, and cells with less than 300 or more than 7000 features were filtered. Then, cells with mitochondrial RNA percentage >20 or with ribosome RNA percentage <5 were further removed. The samples were integrated and were performed normalized, scaled, and PCA analysis through the merge function. The harmony package was employed to evaluate and remove the batch effect in each subgroup [77]. The FindAllMarkers function was used to identify the marker genes of each cluster. The final dataset was performed dimensionality reduction clustering by using the UMAP package [78]. Based on the expression of CAFs markers, *ACTA2*, *FAP*, *PDGFRA*, *PDGFRB*, *PDPN*, *THY1*, and *COL1A1*, the ssGSEA package [79] was used to assess the content of CAFs in transcript samples.

4.8. qRT-PCR

The human gastric mucosa epithelial cell GES-1 and the five GC cell lines (N87, SGC7901, MKN45, AGS, and MGC803) were supplied from The Type Culture Collection of the Chinese Academy of Medical Science. All cultures were incubated in a humidified atmosphere of 5 % CO_2 at 37 °C. TRIzol (Thermo Fisher Scientific Inc) was applied to extract total RNA from cells and a reverse transcription kit (Thermo Fisher Scientific Inc) was used to reverse-transcribe total RNA into cDNA. The expression of GAPDH was taken as a control, and the relative expression of the target genes was calculated using $2^{-\Delta\Delta CT}$. Primer sequences can be seen in Supplementary Table S1.

4.9. RNA interference

Various siRNAs (si-APOD-460, si-APOD-282, si-APOD-539, si-PPP1R14A-340, si-PPP1R14A-183, si-PPP1R14A-69, si-SGCE-326, si-SGCE-1114, and si-SGCE-455) from Gemma Gene were employed to suppress the expression of *APOD*, *PPP1R14A*, and *SGCE*. A scrambled siRNA (si-NC) served as the negative control. The sequences of the siRNAs are provided in Supplementary Table S2. Cells were transiently transfected with 100 pmol of siRNA using polyethylenimine (MCE). After 24 h of transfection, cells were harvested for subsequent experiments.

4.10. CCK8 assay

AGS and SGC-7901 cells were seeded at a density of 2×10^3 cells per well and then incubated overnight on 96-well plates. Subsequent to overnight incubation, each well underwent treatment with 10 μl of CCK-8 solution (# MA0218, MeiluBio, China) for a duration of 1 h. The optical density (OD) values of the cells were subsequently measured using a microplate reader (#ST-360, Kehua Bio-engineering Co., China) at a wavelength of 450 nm. This procedure was replicated for three consecutive days to ascertain the OD values.

4.11. Wound-healing migration assay

In a 6-well plate, approximately 6×10^5 cells were cultured. Upon the formation of a monolayer, the cells were gently scraped using a sterile pipette tip. The cells were washed with PBS to eliminate the scraped cells and were further cultured in a cell culture incubator set at 37 °C and 5 % CO_2 for a duration of 24 h. Microscopic images were captured during this period.

4.12. Colony formation assay

The proliferative capacity of the cells was also tested by colony formation assay. 2×10^3 cells were seeded and cultured for a period of 10–14 days on 6-well plates. The cells were fixed with 4 % paraformaldehyde (#30,188,928, Sinopharm, China) and stained with crystal violet staining buffer (#C0121 -100 ml, Beyotime, China) for counting the cell colonies.

4.13. Western blotting

Cell or animal samples were lysed using cold RIPA lysis buffer (# PC101, Epizyme, China), and the quantification of the extracted proteins was performed using the Pierce BCA protein assay kit (#P0009, Beyotime, China). Following electrophoresis on a sodium dodecyl sulfate polyacrylamide gel (SDS-PAGE), the blots were transferred to an NT nitrocellulose (NC) membrane (# 69924861, Pall Corporation, America). Subsequently, the membrane was incubated in 5 % skim milk for 1 h at room temperature (22–25 °C) and then utilized with primary antibodies: anti-APOD (1:2000, #DF7987, Affinity, Australia), anti-SGCE (1: 1000, #DF7279, Affinity, Australia), anti-PPP1R14A (1:1000, # AF6473, Affinity, Australia), anti-E-cadherin (1:1000, # BF0219, Affinity, Australia), anti-N-

cadherin (1:1000; # 13116T, Cell Signaling Technology, United States), anti-beta-catenin (1:1000, #ET1601-5, HuaBio, China) and anti-beta-actin (1:10,000, #66009-1-1g, Proteintech, China) overnight incubation at 4 °C. Secondary goat anti-rabbit or anti-mouse IgG antibodies (1:10,000, Zhongshan Jin Qiao, China) were applied for 1 h at room temperature (22–25 °C) and illuminated by enhanced chemiluminescence reagent (# MA01862, MeiluBio, China). The integrated optical density of each band was measured using Image-Pro Plus 6.0 software. The relative protein expression level of the target was calculated using beta-actin as a control.

4.14. Statistical analysis

All statistical analyses were completed by R software 4.1.3 [80]. The Spearman correlation analyses were applied to determine the correlation, and $P < 0.05$ was considered statistically significant [81]. Kaplan-Meier method using a two-sided log-rank test was applied for survival analysis of different risk subgroups [82]. The Wilcoxon signed-rank test was employed to compare the two groups' differences, and $P < 0.05$ was the threshold of significance [83].

Data availability statement

The data used in this study is available in the TCGA (http://tcga.cancer.gov/dataportal) portals and the Gene Expression Omnibus (GEO) online database (GSE84437 and GSE163558). Our analyses' protocols and raw figures or other information related to our study could be asked from the corresponding author on reasonable request. Any custom code or mathematical algorithm was not applied in our study and all of the relevant R code or software used has been introduced in the Methods section. Moreover, the code for analysis can be accessible at https://github.com/huijuanwen/GC.

Ethics statement

None.

CRediT authorship contribution statement

Huijuan Wen: Writing – review & editing, Writing – original draft, Project administration, Methodology, Investigation, Data curation, Conceptualization. **Yang Mi:** Writing – original draft, Data curation. **Fazhan Li:** Writing – original draft, Data curation. **Xia Xue:** Writing – review & editing, Writing – original draft, Data curation. **Xiangdong Sun:** Writing – review & editing. **Pengyuan Zheng:** Writing – review & editing, Supervision, Conceptualization. **Simeng Liu:** Writing – original draft, Project administration, Methodology, Investigation, Data curation, Conceptualization.

Declaration of competing interest

The authors declare that they have no known competing financial interests or personal relationships that could have appeared to influence the work reported in this paper.

Acknowledgments

This work was supported by Key projects of discipline construction in Zhengzhou University (No. XKZDJC202001); National Key Research and Development Program in China (No. 2020YFC2006100); Zhengzhou Major Collaborative Innovation Project (No. 18XTZX12003); and for this study, Simeng Liu also received financial support from the Preferential Scientific Research Funds for Overseas Chinese Students in 2020.

Appendix A. Supplementary data

Supplementary data to this article can be found online at https://doi.org/10.1016/j.heliyon.2024.e38823.

References

[1] H. Sung, J. Ferlay, R.L. Siegel, M. Laversanne, I. Soerjomataram, A. Jemal, et al., Global cancer statistics 2020: GLOBOCAN estimates of incidence and mortality worldwide for 36 cancers in 185 countries, CA Cancer J Clin 71 (3) (2021) 209–249.
[2] J. Ferlay, M. Colombet, I. Soerjomataram, D.M. Parkin, M. Pineros, A. Znaor, et al., Cancer statistics for the year 2020: an overview, Int. J. Cancer 149 (4) (2021) 778–789.
[3] E.C. Smyth, M. Nilsson, H.I. Grabsch, N.C. van Grieken, F. Lordick, Gastric cancer, Lancet 396 (10251) (2020) 635–648.
[4] G.B. Baretton, D.E. Aust, Current biomarkers for gastric cancer, Pathologe 38 (2) (2017) 93–97.
[5] M. Ilic, I. Ilic, Epidemiology of stomach cancer, World J. Gastroenterol. 28 (12) (2022) 1187–1203.
[6] T. Matsuoka, M. Yashiro, Biomarkers of gastric cancer: current topics and future perspective, World J. Gastroenterol. 24 (26) (2018) 2818–2832.
[7] Z. Wang, T.M. Mo, L. Tian, J.Q. Chen, Gastrin-17 combined with CEA, CA12-5 and CA19-9 improves the sensitivity for the diagnosis of gastric cancer, Int. J. Gen. Med. 14 (2021) 8087–8095.

[8] W. Wang, X.L. Chen, S.Y. Zhao, Y.H. Xu, W.H. Zhang, K. Liu, et al., Prognostic significance of preoperative serum CA125, CA19-9 and CEA in gastric carcinoma, Oncotarget 7 (23) (2016) 35423–35436.
[9] F. Feng, Y. Tian, G. Xu, Z. Liu, S. Liu, G. Zheng, et al., Diagnostic and prognostic value of CEA, CA19-9, AFP and CA125 for early gastric cancer, BMC Cancer 17 (1) (2017) 737.
[10] H. Shimada, T. Noie, M. Ohashi, K. Oba, Y. Takahashi, Clinical significance of serum tumor markers for gastric cancer: a systematic review of literature by the Task Force of the Japanese Gastric Cancer Association, Gastric Cancer 17 (1) (2014) 26–33.
[11] O. Warburg, On respiratory impairment in cancer cells, Science 124 (3215) (1956) 269–270.
[12] A. Garten, S. Schuster, M. Penke, T. Gorski, T. de Giorgis, W. Kiess, Physiological and pathophysiological roles of NAMPT and NAD metabolism, Nat. Rev. Endocrinol. 11 (9) (2015) 535–546.
[13] A. Chiarugi, C. Dolle, R. Felici, M. Ziegler, The NAD metabolome–a key determinant of cancer cell biology, Nat. Rev. Cancer 12 (11) (2012) 741–752.
[14] S.J. Yang, J.M. Choi, L. Kim, S.E. Park, E.J. Rhee, W.Y. Lee, et al., Nicotinamide improves glucose metabolism and affects the hepatic NAD-sirtuin pathway in a rodent model of obesity and type 2 diabetes, J. Nutr. Biochem. 25 (1) (2014) 66–72.
[15] C.F. Lee, J.D. Chavez, L. Garcia-Menendez, Y. Choi, N.D. Roe, Y.A. Chiao, et al., Normalization of NAD+ redox balance as a therapy for heart failure, Circulation 134 (12) (2016) 883–894.
[16] L. Rajman, K. Chwalek, D.A. Sinclair, Therapeutic potential of NAD-boosting molecules: the in vivo evidence, Cell Metab 27 (3) (2018) 529–547.
[17] G.M. Shah, R.G. Shah, H. Veillette, J.B. Kirkland, J.L. Pasieka, R.R. Warner, Biochemical assessment of niacin deficiency among carcinoid cancer patients, Am. J. Gastroenterol. 100 (10) (2005) 2307–2314.
[18] D.S. Clement, M.E. Tesselaar, M.E. van Leerdam, R. Srirajaskanthan, J.K. Ramage, Nutritional and vitamin status in patients with neuroendocrine neoplasms, World J. Gastroenterol. 25 (10) (2019) 1171–1184.
[19] G. Bouma, M. van Faassen, G. Kats-Ugurlu, E.G. de Vries, I.P. Kema, A.M. Walenkamp, Niacin (vitamin B3) supplementation in patients with serotonin-producing neuroendocrine tumor, Neuroendocrinology 103 (5) (2016) 489–494.
[20] A.A. Pramono, G.M. Rather, H. Herman, K. Lestari, J.R. Bertino, NAD- and NADPH-contributing enzymes as therapeutic targets in cancer: an overview, Biomolecules 10 (3) (2020).
[21] S. Falzoni, G. Donvito, F. Di Virgilio, Detecting adenosine triphosphate in the pericellular space, Interface Focus 3 (3) (2013) 20120101.
[22] N. Xie, L. Zhang, W. Gao, C. Huang, P.E. Huber, X. Zhou, et al., NAD(+) metabolism: pathophysiologic mechanisms and therapeutic potential, Signal Transduct Target Ther 5 (1) (2020) 227.
[23] C. Li, Y. Zhu, W. Chen, M. Li, M. Yang, Z. Shen, et al., Circulating NAD+ metabolism-derived genes unveils prognostic and peripheral immune infiltration in amyotrophic lateral sclerosis, Front. Cell Dev. Biol. 10 (2022) 831273.
[24] Y. Wang, F. Song, X. Zhang, C. Yang, Mitochondrial-related transcriptome feature correlates with prognosis, vascular invasion, tumor microenvironment, and treatment response in hepatocellular carcinoma, Oxid. Med. Cell. Longev. 2022 (2022) 1592905.
[25] L. Lin, L. Chen, Z. Xie, J. Chen, L. Li, A. Lin, Identification of NAD(+) metabolism-derived gene signatures in ovarian cancer prognosis and immunotherapy, Front. Genet. 13 (2022) 905238.
[26] X. Lei, Y. Lei, J.K. Li, W.X. Du, R.G. Li, J. Yang, et al., Immune cells within the tumor microenvironment: biological functions and roles in cancer immunotherapy, Cancer Lett. 470 (2020) 126–133.
[27] N. Grunberg, M. Pevsner-Fischer, T. Goshen-Lago, J. Diment, Y. Stein, H. Lavon, et al., Cancer-associated fibroblasts promote aggressive gastric cancer phenotypes via heat shock factor 1-mediated secretion of extracellular vesicles, Cancer Res. 81 (7) (2021) 1639–1653.
[28] R. Peng, S. Liu, W. You, Y. Huang, C. Hu, Y. Gao, et al., Gastric microbiome alterations are associated with decreased CD8+ tissue-resident memory T cells in the tumor microenvironment of gastric cancer, Cancer Immunol. Res. 10 (10) (2022) 1224–1240.
[29] P.P. Desai, C.H. Bunker, F.A. Ukoli, M.I. Kamboh, Genetic variation in the apolipoprotein D gene among African blacks and its significance in lipid metabolism, Atherosclerosis 163 (2) (2002) 329–338.
[30] T. Utsunomiya, K. Ogawa, K. Yoshinaga, M. Ohta, K. Yamashita, K. Mimori, et al., Clinicopathologic and prognostic values of apolipoprotein D alterations in hepatocellular carcinoma, Int. J. Cancer 116 (1) (2005) 105–109.
[31] K. Ogawa, T. Utsunomiya, K. Mimori, K. Yamashita, M. Okamoto, F. Tanaka, et al., Genomic screens for genes upregulated by demethylation in colorectal cancer: possible usefulness for clinical application, Int. J. Oncol. 27 (2) (2005) 417–426.
[32] J. Vazquez, L. Gonzalez, A. Merino, F. Vizoso, Expression and clinical significance of apolipoprotein D in epithelial ovarian carcinomas, Gynecol. Oncol. 76 (3) (2000) 340–347.
[33] I. Diez-Itza, F. Vizoso, A.M. Merino, L.M. Sanchez, J. Tolivia, J. Fernandez, et al., Expression and prognostic significance of apolipoprotein D in breast cancer, Am. J. Pathol. 144 (2) (1994) 310–320.
[34] R.B. Hamanaka, N.S. Chandel, Cell biology. Warburg effect and redox balance, Science 334 (6060) (2011) 1219–1220.
[35] D. Anastasiou, G. Poulogiannis, J.M. Asara, M.B. Boxer, J.K. Jiang, M. Shen, et al., Inhibition of pyruvate kinase M2 by reactive oxygen species contributes to cellular antioxidant responses, Science 334 (6060) (2011) 1278–1283.
[36] J.Y. Sung, J.H. Cheong, The matrisome is associated with metabolic reprograming in stem-like phenotypes of gastric cancer, Cancers 14 (6) (2022).
[37] H. Xu, H. Wan, M. Zhu, L. Feng, H. Zhang, F. Su, Discovery and validation of an epithelial-mesenchymal transition-based signature in gastric cancer by genomics and prognosis analysis, BioMed Res. Int. 2021 (2021) 9026918.
[38] T.K. Mak, X. Li, H. Huang, K. Wu, Z. Huang, Y. He, et al., The cancer-associated fibroblast-related signature predicts prognosis and indicates immune microenvironment infiltration in gastric cancer, Front. Immunol. 13 (2022) 951214.
[39] S. Xue, T. Zheng, J. Yan, J. Ma, C. Lin, S. Dong, et al., Identification of a 3-gene model as prognostic biomarker in patients with gastric cancer, Front. Oncol. 12 (2022) 930586.
[40] M.E. Fiori, S. Di Franco, L. Villanova, P. Bianca, G. Stassi, R. De Maria, Cancer-associated fibroblasts as abettors of tumor progression at the crossroads of EMT and therapy resistance, Mol. Cancer 18 (1) (2019) 70.
[41] H. Kobayashi, A. Enomoto, S.L. Woods, A.D. Burt, M. Takahashi, D.L. Worthley, Cancer-associated fibroblasts in gastrointestinal cancer, Nat. Rev. Gastroenterol. Hepatol. 16 (5) (2019) 282–295.
[42] E. Helms, M.K. Onate, M.H. Sherman, Fibroblast heterogeneity in the pancreatic tumor microenvironment, Cancer Discov. 10 (5) (2020) 648–656.
[43] D. Ostroumov, N. Fekete-Drimusz, M. Saborowski, F. Kuhnel, N. Woller, CD4 and CD8 T lymphocyte interplay in controlling tumor growth, Cell. Mol. Life Sci. 75 (4) (2018) 689–713.
[44] Z. Wu, F. Zhang, Y. Wang, Z. Lu, C. Lin, Identification and validation of the lncRNA MYOSLID as a regulating factor of necroptosis and immune cell infiltration in colorectal cancer following necroptosis-related LncRNA model establishment, Cancers 14 (18) (2022).
[45] D. Dai, B. Chen, Y. Feng, W. Wang, Y. Jiang, H. Huang, et al., Prognostic value of prostaglandin I2 synthase and its correlation with tumor-infiltrating immune cells in lung cancer, ovarian cancer, and gastric cancer, Aging (Albany NY) 12 (10) (2020) 9658–9685.
[46] K. Narci, D.C. Kahraman, A. Koyas, T. Ersahin, N. Tuncbag, R.C. Atalay, Context dependent isoform specific PI3K inhibition confers drug resistance in hepatocellular carcinoma cells, BMC Cancer 22 (1) (2022) 320.
[47] J. Wu, Y. Wei, T. Li, L. Lin, Z. Yang, L. Ye, DNA methylation-mediated lowly expressed AOX1 promotes cell migration and invasion of prostate cancer, Urol. Int. (2022) 1–9.
[48] L. Xiong, Y. Feng, W. Hu, J. Tan, S. Li, H. Wang, Expression of AOX1 predicts prognosis of clear cell renal cell carcinoma, Front. Genet. 12 (2021) 683173.
[49] A. Rizzo, A.D. Ricci, G. Brandi, PD-L1, TMB, MSI, and other predictors of response to immune checkpoint inhibitors in biliary tract cancer, Cancers 13 (3) (2021).
[50] D.P. Carbone, M. Reck, L. Paz-Ares, B. Creelan, L. Horn, M. Steins, et al., First-line nivolumab in stage IV or recurrent non-small-cell lung cancer, N. Engl. J. Med. 376 (25) (2017) 2415–2426.

[51] F. Pietrantonio, R. Miceli, A. Raimondi, Y.W. Kim, W.K. Kang, R.E. Langley, et al., Individual patient data meta-analysis of the value of microsatellite instability as a biomarker in gastric cancer, J. Clin. Oncol. 37 (35) (2019) 3392–3400.
[52] D. Mao, Z. Zhou, S. Song, D. Li, Y. He, Z. Wei, et al., Identification of stemness characteristics associated with the immune microenvironment and prognosis in gastric cancer, Front. Oncol. 11 (2021) 626961.
[53] B.J. van Denderen, E.W. Thompson, Cancer: the to and fro of tumour spread, Nature 493 (7433) (2013) 487–488.
[54] X. Ye, R.A. Weinberg, Epithelial-mesenchymal plasticity: a central regulator of cancer progression, Trends Cell Biol. 25 (11) (2015) 675–686.
[55] G.P. Wagner, K. Kin, V.J. Lynch, Measurement of mRNA abundance using RNA-seq data: RPKM measure is inconsistent among samples, Theory Biosci 131 (4) (2012) 281–285.
[56] S.J. Yoon, J. Park, Y. Shin, Y. Choi, S.W. Park, S.G. Kang, et al., Deconvolution of diffuse gastric cancer and the suppression of CD34 on the BALB/c nude mice model, BMC Cancer 20 (1) (2020) 314.
[57] J. Wang, S. Cong, H. Wu, Y. He, X. Liu, L. Sun, et al., Identification and analysis of potential autophagy-related biomarkers in endometriosis by WGCNA, Front. Mol. Biosci. 8 (2021) 743012.
[58] S. Chen, D. Yang, C. Lei, Y. Li, X. Sun, M. Chen, et al., Identification of crucial genes in abdominal aortic aneurysm by WGCNA, PeerJ 7 (2019) e7873.
[59] H. Jiang, D. Yu, P. Yang, R. Guo, M. Kong, Y. Gao, et al., Revealing the transcriptional heterogeneity of organ-specific metastasis in human gastric cancer using single-cell RNA Sequencing, Clin. Transl. Med. 12 (2) (2022) e730.
[60] X. Hu, S. Ni, K. Zhao, J. Qian, Y. Duan, Bioinformatics-led discovery of osteoarthritis biomarkers and inflammatory infiltrates, Front. Immunol. 13 (2022) 871008.
[61] Q. Cheng, L. Wang, LncRNA XIST serves as a ceRNA to regulate the expression of ASF1A, BRWD1M, and PFKFB2 in kidney transplant acute kidney injury via sponging hsa-miR-212-3p and hsa-miR-122-5p, Cell Cycle 19 (3) (2020) 290–299.
[62] M.D. Wilkerson, D.N. Hayes, ConsensusClusterPlus: a class discovery tool with confidence assessments and item tracking, Bioinformatics 26 (12) (2010) 1572–1573.
[63] R.S. Zhou, E.X. Zhang, Q.F. Sun, Z.J. Ye, J.W. Liu, D.H. Zhou, et al., Integrated analysis of lncRNA-miRNA-mRNA ceRNA network in squamous cell carcinoma of tongue, BMC Cancer 19 (1) (2019) 779.
[64] S. Hanzelmann, R. Castelo, J. Guinney, GSVA: gene set variation analysis for microarray and RNA-seq data, BMC Bioinf. 14 (2013) 7.
[65] J. Liu, J. Li, H. Li, A. Li, B. Liu, L. Han, A comprehensive analysis of candidate genes and pathways in pancreatic cancer, Tumour Biol 36 (3) (2015) 1849–1857.
[66] S. Zhang, Z. Wu, J. Xie, Y. Yang, L. Wang, H. Qiu, DNA methylation exploration for ARDS: a multi-omics and multi-microarray interrelated analysis, J. Transl. Med. 17 (1) (2019) 345.
[67] M. Pierre-Jean, F. Mauger, J.F. Deleuze, E. Le Floch, PIntMF: penalized integrative matrix factorization method for multi-omics data, Bioinformatics 38 (4) (2021) 900–907.
[68] Y. Fang, S. Huang, L. Han, S. Wang, B. Xiong, Comprehensive analysis of peritoneal metastasis sequencing data to identify LINC00924 as a prognostic biomarker in gastric cancer, Cancer Manag. Res. 13 (2021) 5599–5611.
[69] P. Charoentong, F. Finotello, M. Angelova, C. Mayer, M. Efremova, D. Rieder, et al., Pan-cancer immunogenomic analyses reveal genotype-immunophenotype relationships and predictors of response to checkpoint blockade, Cell Rep. 18 (1) (2017) 248–262.
[70] K. Zhao, Z. Ma, W. Zhang, Comprehensive analysis to identify SPP1 as a prognostic biomarker in cervical cancer, Front. Genet. 12 (2021) 732822.
[71] E.K. Gustavsson, D. Zhang, R.H. Reynolds, S. Garcia-Ruiz, M. Ryten, ggtranscript: an R package for the visualization and interpretation of transcript isoforms using ggplot2, Bioinformatics 38 (15) (2022) 3844–3846.
[72] S. Zhou, H. Lu, M. Xiong, Identifying immune cell infiltration and effective diagnostic biomarkers in rheumatoid arthritis by bioinformatics analysis, Front. Immunol. 12 (2021) 726747.
[73] D. Jia, S. Li, D. Li, H. Xue, D. Yang, Y. Liu, Mining TCGA database for genes of prognostic value in glioblastoma microenvironment, Aging (Albany NY) 10 (4) (2018) 592–605.
[74] A. Mayakonda, D.C. Lin, Y. Assenov, C. Plass, H.P. Koeffler, Maftools: efficient and comprehensive analysis of somatic variants in cancer, Genome Res. 28 (11) (2018) 1747–1756.
[75] T.M. Malta, A. Sokolov, A.J. Gentles, T. Burzykowski, L. Poisson, J.N. Weinstein, et al., Machine learning identifies stemness features associated with oncogenic dedifferentiation, Cell 173 (2) (2018) 338–354 e315.
[76] T. Stuart, A. Butler, P. Hoffman, C. Hafemeister, E. Papalexi, W.M. Mauck 3rd, et al., Comprehensive integration of single-cell data, Cell 177 (7) (2019) 1888–1902 e1821.
[77] I. Korsunsky, N. Millard, J. Fan, K. Slowikowski, F. Zhang, K. Wei, et al., Fast, sensitive and accurate integration of single-cell data with Harmony, Nat. Methods 16 (12) (2019) 1289–1296.
[78] E. Gralinska, C. Kohl, B. Sokhandan Fadakar, M. Vingron, Visualizing cluster-specific genes from single-cell transcriptomics data using association plots, J. Mol. Biol. 434 (11) (2022) 167525.
[79] L. Liang, J. Yu, J. Li, N. Li, J. Liu, L. Xiu, et al., Integration of scRNA-seq and bulk RNA-seq to analyse the heterogeneity of ovarian cancer immune cells and establish a molecular risk model, Front. Oncol. 11 (2021) 711020.
[80] B.H. Chang, D.C. Hoaglin, Meta-analysis of odds ratios: current good practices, Med Care 55 (4) (2017) 328–335.
[81] P. Ecaterina, P. Valeriana, B. Djina, T. Olga, Glutathione-related antioxidant defense system in patients with hypertensive retinopathy, Rom J Ophthalmol 65 (1) (2021) 46–53.
[82] D.G. Vossler, S. Knake, T.J. O'Brien, M. Watanabe, M. Brock, B. Steiniger-Brach, et al., Efficacy and safety of adjunctive lacosamide in the treatment of primary generalised tonic-clonic seizures: a double-blind, randomised, placebo-controlled trial, J. Neurol. Neurosurg. Psychiatry 91 (10) (2020) 1067–1075.
[83] X. Li, Y. Wu, M. Wei, Y. Guo, Z. Yu, H. Wang, et al., A novel index of functional connectivity: phase lag based on Wilcoxon signed rank test, Cogn Neurodyn 15 (4) (2021) 621–636.